Loughborough University

This item was submitted to Loughborough's Research Repository by the author.
Items in Figshare are protected by copyright, with all rights reserved, unless otherwise indicated.

Low-cycle fatigue of single crystal nickel-based superalloy – mechanical testing and TEM characterisation

PLEASE CITE THE PUBLISHED VERSION

https://doi.org/10.1016/j.msea.2018.12.084

PUBLISHER

© 2018 The Author(s). Published by Elsevier B.V.

VERSION

VoR (Version of Record)

PUBLISHER STATEMENT

This work is made available according to the conditions of the Creative Commons Attribution 4.0 International (CC BY 4.0) licence. Full details of this licence are available at: http://creativecommons.org/licenses/ by/4.0/

LICENCE

CC BY 4.0

REPOSITORY RECORD

Zhang, Lu, Liguo Zhao, Anish Roy, Vadim Silberschmidt, and G. McColvin. 2019. “Low-cycle Fatigue of Single Crystal Nickel-based Superalloy – Mechanical Testing and TEM Characterisation”. figshare. https://hdl.handle.net/2134/36489.

Materials Science & Engineering A 744 (2019) 538–547

Contents lists available at ScienceDirect

Materials Science & Engineering A

journal homepage: www.elsevier.com/locate/msea

Low-cycle fatigue of single crystal nickel-based superalloy – mechanical testing and TEM characterisation

L. Zhang[a], LG. Zhao[a,*], A. Roy[a], VV. Silberschmidt[a], G. McColvin[b]

[a] Wolfson School of Mechanical, Electrical and Manufacturing Engineering, Loughborough University, Loughborough, LE11 3TU, UK
[b] GE Power, Rugby, CV21 2NH, UK

ARTICLE INFO

Keywords:
Low-cycle fatigue
Cyclic hardening
Cyclic-softening
TEM
Dislocations
Single crystal

ABSTRACT

Low-cycle fatigue (LCF) is studied for a nickel-based single-crystal superalloy in this paper, with a focus on the effect of crystal orientation and temperature. Specifically, cyclic deformation of the alloy was compared for [001]- and [111]-oriented samples tested under strain-controlled conditions at room temperature and 825 °C. Either cyclic hardening or softening was observed during the LCF process, depending on the strain amplitude, crystallographic orientation and temperature. LCF life was also reduced significantly by changing loading orientation from [001] to [111] or increasing temperature to 825 °C. Employing a comprehensive study with transmission electron microscopy (TEM), a connection between microstructure and mechanical behaviour of the alloy is discussed. It was found that the processes of γ′-precipitate dissolution and dislocation recovery were responsible for cyclic softening. Alignments and pile-ups of dislocations in the γ matrix, which prohibited their movement and reduced the interaction of dislocations on different slip systems, contributed to cyclic hardening.

1. Introduction

Nickel-based superalloys are extensively used for manufacture of rotating discs and blades of gas turbine engines due to their excellent mechanical properties at high temperatures [1]. Nickel-based single-crystal superalloys, with coherent two-phase microstructure (γ′ precipitates and γ matrix), are preferred for turbine blades operating at temperatures up to 850 °C because of their superior creep resistance, a result of the absence of grain boundaries. The Ni_3Al γ′-precipitate phase is formed of cuboidal particles, regularly distributed in the γ matrix phase, with a volume fraction up to 70%. These alloys are inherently anisotropic, and their mechanical responses depend on the orientation of the loading direction with regard to the microstructural crystallographic axes [2].

Typically, gas turbines operate at high alternating load for a prolonged time, leading to fatigue damage. Extensive research was carried out to study both monotonic deformation and low-cycle fatigue (LCF) life of single-crystal nickel superalloys, especially the influence of crystallographic orientation and temperature on structural integrity of components. Segersäll and Moverare [3] investigated both tensile and compressive yielding behaviours of a nickel-based single-crystal superalloy along [001, 011] and [111] orientations at 500 °C. Visible deformation bands were only observed for the [011] orientation. Also, the highest Young's modulus was obtained for the [111] orientation, with the lowest one being in the [001] direction. Fleury and Remy [4] reported cyclic softening behaviour for AM1 alloy tested at elevated temperature for varied orientations; the softening effect reduced with a decrease in strain amplitude. Li et al. [5] investigated the LCF deformation of DD6 alloy at 980 °C and observed the cyclic hardening effect for [001] orientation. In [011] and [111] orientations, the studied alloy demonstrated cyclic softening or a stabilised stress amplitude under low strain amplitude, with a transition to cyclic hardening at high amplitude. Liu et al. [6] studied a Re-containing nickel-based single-crystal superalloy under LCF at 980 °C, and reported that the [001]-oriented alloy exhibited cyclic softening, irrespective of the strain amplitude applied. While the [011]- and [111]-oriented alloy demonstrated cyclic hardening under low strain amplitude and cyclic softening under high strain amplitude. Sundararaman et al. [7] observed softening behaviour of a nickel-based superalloy Nimonic PE16 subjected to LCF at room temperature under LCF conditions, and the dislocations were restricted to move within thin slip bands, parallel to the {111} planes. Raman and Padmanabhan [8] studied the strain-controlled LCF behaviour of Nimonic 90 at room temperature. They found that the initial cyclic hardening was caused by formation of slip bands, and the cyclic softening was a result of the shearing of the γ′ precipitates by dislocations. Petrenec et al. [9] observed highly inhomogeneous planar dislocation structures in INCONEL 713 LC superalloy after fatigue deformation at temperatures up to 800 °C. However,

* Corresponding author.
E-mail address: L.Zhao@lboro.ac.uk (L. Zhao).

https://doi.org/10.1016/j.msea.2018.12.084
Received 15 November 2018; Received in revised form 15 December 2018; Accepted 17 December 2018
Available online 18 December 2018
0921-5093/ © 2018 The Author(s). Published by Elsevier B.V. This is an open access article under the CC BY license (http://creativecommons.org/licenses/BY/4.0/).

Pineau and Antolovich [10] reported that the dislocation arrangement became homogeneous with the increase of temperature and the density of dislocations in the slip bands was much lower than that at ambient temperature. At a temperature above 800 °C, the homogenous non-planar slip became dominant, and there were no slip bands observed. Chu et al. [11] compared the LCF behaviour of Ni-based superalloy DZ951 at 700 °C and 900 °C, and reported the formation of slip bands, running through the γ′ precipitates, at 700 °C but not at 900 °C. Volker and Monika [12] suggested that, at 700 °C, Orowan looping was the mechanism controlling the LCF deformation, and the dislocation loops were formed by cross slip of dislocations in the horizontal γ channels. In addition, Yu et al. [13] found that dislocation climb, cross slip and interaction between dislocation and carbides were the main deformation mechanisms for the SRR99 alloy under LCF at 900 °C. These studies clearly demonstrate a strong dependency of LCF behaviour of nickel single-crystal alloys on crystallographic orientation and temperature.

To reveal the underlying deformation mechanism of nickel alloys, TEM was extensively utilised to characterise the evolution of dislocations and other crystal defects such as stacking faults and twin/grain boundaries after mechanical tests. Gabb and Welsch [14] reported generation and rearrangement of dislocations in [001]- and [$\bar{1}$11]-oriented specimens after LCF tests at 1050 °C. The dislocations were distributed homogeneously, with no observation of slip bands. The dislocations were mainly restricted to the γ phase, especially accumulated at the γ/γ′ interfaces that led to a cyclic softening effect. Wang et al. [15] studied the deformation mechanisms of a nickel-based single-crystal superalloy during LCF at various temperatures (RT, 760 °C, 900 °C and 980 °C). They observed the cross-slip of dislocations in the γ matrix during the LCF tests at 760 °C and 900 °C, which was an important component of the slip bands formed at 900 °C. Li and Ping [16] found that the fatigue life for nickel-base single-crystal superalloy increased with a decreasing strain amplitude based on LCF tests at 760 °C and 870 °C. By evaluating the dislocation characteristics with TEM, they concluded that the homogeneous distribution of secondary γ'-particles in the γ matrix contributed to enhancement of fatigue resistance. The formation of persistent slip bands (PSBs) induced the initiation of fatigue crack and the crack growth along the PSBs. At 870 °C and higher strain amplitude, the tangling of dislocations and progressive coarsening of precipitates led to higher local stress concentration, which promoted early fatigue crack initiation.

Most existing work on LCF of single-crystal nickel alloys was dedicated to the effect of either temperature or orientation, and there is a lack of comparative studies by varying both temperature and orientation. In this study, LCF tests were performed to investigate cyclic deformation of a single-crystal nickel-based superalloy MD2 along [001] and [111] orientations at both room temperature and 825 °C (working temperature of turbine blades). The material is newly developed by Alstom Power (now GE power) and contains no Rhenium. Experimental studies, as well as microstructure characterisation, are particularly needed in order to provide a better understanding of the alloy's fatigue behaviour. Here, cyclic stress-strain responses and fatigue life were analysed based on the LCF tests with varied orientation and temperature. SEM and TEM were used to characterize the fracture surfaces and dislocation microstructures in the γ-matrix and γ'-precipitates, respectively, after LCF testing.

2. LCF tests and microscopic characterisation

2.1. Material and specimens

The material studied is a third-generation nickel-based single-crystal superalloy G-Ni 135SX (MD2), with a chemical composition of Ni-5.1Co-6.0Ta-8.0Cr-8.1W-5.0Al-1.3Ti-2.1Mo-0.1Hf-0.1Si (in wt%). This alloy was recently developed by Alstom Power (now GE power) for industrial gas-turbine applications and contains no rhenium. Single-crystal rods were manufactured in two orientations ([001] and [111]) employing a casting process. A solution heat treatment (8 h at 1285 °C) and a two-stage precipitation hardening treatment (6 h at 1080 °C and 16 h at 870 °C) in argon and vacuum were performed. Specimens used for LCF tests were machined from the single-crystal rods using an electrical-discharge machining (EDM) process, with either [001] or [111] orientation along the loading axis. Each specimen had a cylindrical dog-bone shape with a gauge length of 13 mm and a diameter of 4.37 mm at the gauge section (Fig. 1).

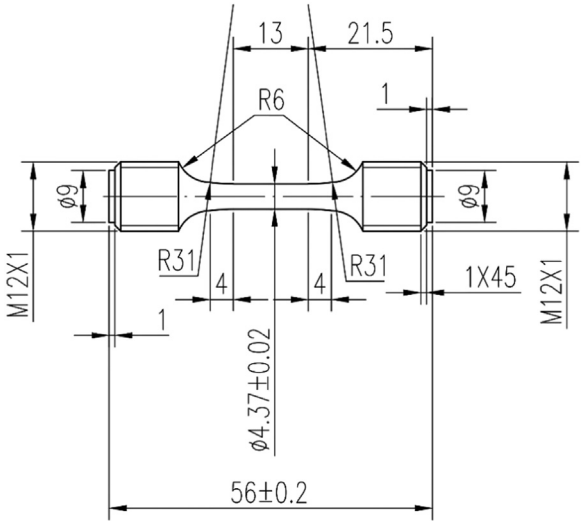


Fig. 1. Geometry of specimens used for low-cycle fatigue tests (all dimensions in mm).

2.2. LCF tests

LCF tests were performed at two different temperatures - room temperature (24 °C) and 825 °C - using a servo-hydraulic testing machine. All tests were strain controlled, with a fully-reversed ($R = -1$) triangular waveform and a strain rate of 0.001/s. Three different strain amplitudes, 0.6% (30 cycles), 0.8% (30 cycles) and 1.0% (till complete fracture), were consecutively applied in each test. Based on our previous experience with this material [17], the chosen strain amplitudes allowed us to study the cyclic deformation of the alloy with varied amount of plastic deformation for both [001] and [111] orientations. For instance, at a strain amplitude of 0.6%, [001]-oriented sample exhibited primarily elastic response and [111]-oriented sample showed small plastic deformation. While at a strain amplitude of 1.0%, both [001]- and [111]-oriented samples showed increased plastic deformation, with a clear development of hysteresis loops. In addition, the stepwise fatigue experiments also allowed us to study the dependence of cyclic hardening/softening on increasing strain amplitude by testing a single sample only, a method used in [18]. This is particularly cost-effective in terms of material and machine usage. Elongation of samples was measured using an extensometer (12 mm gauge length) attached to the gauge section of the specimen. The test matrix is given in Table 1.

2.3. SEM and TEM characterisation

A field emission scanning electron microscope (FE-SEM) JEOL JSM-7800F was used for fractography analysis, with an accelerating voltage of 5 kV, a probe current of 8 nA and a working distance of 18 mm. Foils for TEM analysis were prepared with their plane normal to the loading axis. At first discs with thickness of about 800 μm were cut with EDM at a distance of 3 mm away from the fracture surfaces of the tested specimens. Subsequently, they were ground with SiC abrasive paper of 240, 400, 600, 1200 and 2000 grit sizes to a thickness of less than 50μm and then cut into foils with a diameter of 3 mm. After mechanical

Table 1
LCF test conditions.

Orientation	Temperature	Strain amplitude
[001]	825 °C	0.6% for 30 cycles; 0.8% for 30 cycles; 1.0% till failure
[111]	825 °C	0.6% for 30 cycles; 0.8% (failed at 20 cycles)
[001]	RT	0.6% for 30 cycles; 0.8% for 30 cycles; 1.0% till failure

polishing, the foils were thinned electrochemically in a twin-jet electropolisher with an electrolyte solution consisting of 20% perchloric acid and 80% alcohol under a voltage of 20 V, an electric current of 20 mA and a temperature of −3 °C (using liquid chlorine to decrease the temperature). Microstructural observations were conducted with JEOL JEM-2100 TEM operating at 200 kV; a double-tilt holder was used to rotate the specimens and achieve diffraction patterns for imaging.

3. Results

3.1. LCF behaviour

The first stress-strain loop for each strain amplitude (i.e., 0.6%, 0.8% and 1.0%) is compared in Fig. 2 for the [001]- and [111]-oriented specimens tested at room temperature and 825 °C. The stress amplitude, as a function of the number of cycles, is also compared in Fig. 3 for the three strain amplitudes.

At 825 °C and under the 0.6% strain amplitude, the specimen exhibited an elastic response for the [001] orientation during cyclic loading, with a stress amplitude of around 610 MPa (Fig. 2a). After 30 cycles, the strain amplitude was increased to 0.8%, which led to an increase in stress amplitude (800 MPa; Fig. 2b). An initial cyclic softening was observed, followed by a stabilisation of the stress amplitude at around 768 MPa (Fig. 3b). As the strain amplitude increased to 1.0%, the stress amplitude rose to 912 MPa (Fig. 2c). The area of hysteresis loop also increased, indicating higher plastic deformation of the alloy. Similar to the behaviour at 0.8% strain amplitude, the material exhibited an initial cyclic softening, followed by a long period of saturation in the stress amplitude (Fig. 3). Towards the end of the test, a sharp stress drop was observed because of the initiation and rapid propagation of fatigue crack. At 503 cycles, the specimen experienced a complete fracture (Fig. 3a).

At 825 °C, the results for the [111] orientation are markedly different from those for the [001] orientation (Fig. 2). Under the strain amplitude of 0.6%, plastic deformation can be observed from the well-developed hysteresis loop for the [111] orientation, with a starting stress amplitude of 890 MPa, which was much higher than 610 MPa observed for [001] orientation (Fig. 2a). Different from the [001] orientation, the cyclic stress response for [111] orientation displays an initial cyclic hardening under 0.6% strain amplitude, with a peak stress amplitude of 1020 MPa, which eventually saturated (Fig. 3). When the strain amplitude increased to 0.8% from cycle 30, the stress amplitude increased by 20 MPa (Fig. 3b), i.e., from 1020 MPa to 1040 MPa, which is an order of magnitude smaller than the respective increase observed for the [001] orientation – from 610 MPa to 800 MPa. Under 0.8% strain amplitude, cyclic softening was observed initially which was

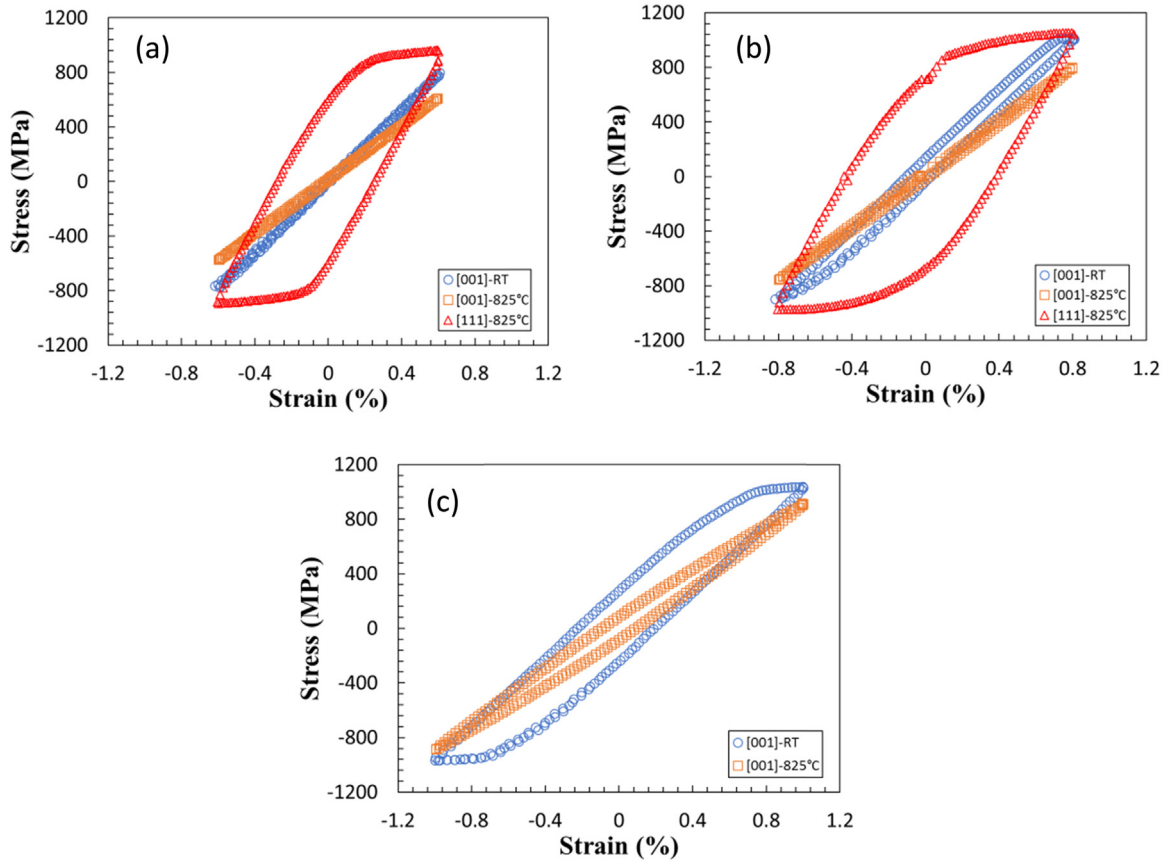


Fig. 2. Stress-strain loops for the first cycle at a strain amplitude of (a) 0.6%, (b) 0.8% and (c) 1.0% for [001]- and [111]-oriented specimens tested at room temperature and 825 °C.

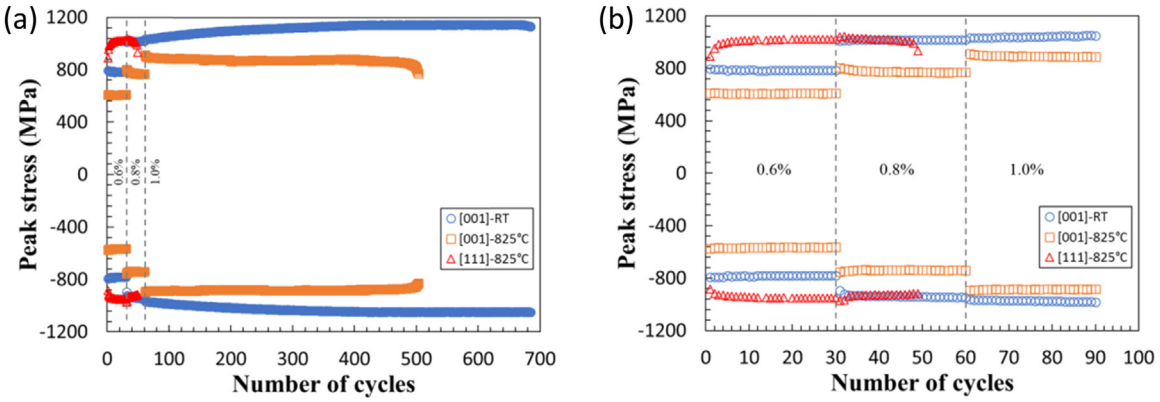


Fig. 3. Stress-evolution to failure for [001]- and [111]-oriented specimens tested at room temperature and 825 °C.

sustained till failure (Fig. 3). Similar to the [001]-oriented specimen, a rapid stress drop occurred before fracture, as a result of crack initiation and the subsequent crack propagation. Also, the specimen with [111] orientation survived just 20 cycles under 0.8% strain amplitude, so could not be tested at a strain level of 1.0%. This gave a total fatigue life of 50 cycles, which is almost ten times shorter than the fatigue life for the [001]-oriented specimen with 503 cycles (Fig. 3a).

At room temperature and under a strain amplitude of 0.6%, the [001]-oriented specimen showed mostly elastic behaviour, similar to that at 825 °C, except for a higher peak stress (790 MPa; Fig. 2a). With an increase in the strain amplitude to 0.8%, the stress amplitude increased to 1010 MPa, much higher than that at 825 °C (Fig. 2b). Besides, the specimen experienced cyclic hardening at the beginning after the stress-amplitude increase with a growing number of cycles, which was in sharp contrast to the initial cyclic softening observed at 825 °C (Fig. 3b). With an increase in the strain amplitude to 1.0%, the increase in stress amplitude was curtailed (an increase from 1020 MPa to 1030 MPa was observed; Fig. 2c), which was significantly smaller than that at 825 °C (768–912 MPa; Fig. 2c). Furthermore, the specimen exhibited continuous cyclic hardening under 1.0% strain amplitude, as opposed to softening behaviour at 825 °C (Fig. 3b). The alloy endured 685 cycles in total before fracture, indicating that the [001]-oriented alloy had a longer fatigue life at room temperature (Fig. 3a).

In addition, it was found that the elastic modulus decreased with the increase in the strain amplitude, by comparing the linear part of the hysteresis loop for different levels of the strain amplitude. This was probably due to the development of defects such as small cracks and micro-pores in the specimen during fatigue deformation exacerbated by the increasing level of applied strain amplitude. According to continuum damage mechanics for uniaxial loading, the evolution of stress σ takes the form:

$$\sigma = (1-\omega)E\varepsilon, \tag{1}$$

where ω is the damage variable ($0 \leq \omega \leq 1$), E is the elastic modulus of the undamaged material and ε is the strain magnitude. As the damage variable ω increases with the number of cycles, the equivalent elastic modulus $\widetilde{E} = (1-\omega)E$ decreases. For each strain amplitude, the equivalent elastic modulus $\widetilde{E}$ was calculated as 99.37 GPa (0.6%), 97.27 GPa (0.8%) and 89.94 GPa (1.0%), indicating an increase of damage variable ω, i.e., 0, 0.021 and 0.075 for 0.6%, 0.8% and 1.0% strain amplitudes, respectively, in the implemented tests.

3.2. Fracture surface analyses

Fracture surfaces of the failed specimens were examined with SEM, and the fractographs are presented in Fig. 4 for all three cases. The fractography showed that the fatigue crack initiated at, or near, the surface of the specimens. After initiation, the crack propagated in the direction either perpendicular to the loading direction (mode I) or along different slip planes (shear- or slip-dominated). Cleavage-like facets were observed, as a result of crack growth along the octahedral slip planes. Micro-pores at the specimen surface might also act as sources of stress concentration, leading to fatigue crack initiation (Fig. 4a). In addition, for the [001]-oriented specimen tested at room temperature, the cleavage facets were larger and less textured with smaller cleavage steps, when compared to the specimen tested at 825 °C

3.3. TEM analyses

TEM images of the as-received alloy are shown in Fig. 5 for both [001] and [111] orientations. Cuboidal γ′ phases with a size of about 0.5 μm were regularly distributed in the γ matrix. The volume fraction of the γ′ precipitates was estimated at 70%. The width of the γ channels was about 70 nm and 120 nm, respectively, when measured along the [001] and [111] orientations in the TEM images. Overall, the alloy was found to be almost free of dislocations, with a few dislocation lines observed for either orientation.

The microstructure including dislocation distribution is shown in Fig. 6 for the [001]-oriented specimen fractured in fatigue at 825 °C. Apparently, the width of γ matrix channel remained the same (compared to as-received sample, Fig. 5), while the corners of γ′ precipitates were dissolved slightly. The dislocations were mainly contained and distributed heterogeneously in the γ-matrix channels (see Fig. 6a). Dislocation tangles were generated when loops of long dislocations bowed out and encountered other dislocations in the γ channel. The dislocation loops demonstrated zig-zag features (Fig. 6b). Also, irregular square-shaped dislocation networks were formed at γ/γ′ interfaces in some regions as marked in Fig. 6b. This indicates that dislocations underwent a re-orientation process, i.e., from ⟨110⟩ to ⟨100⟩ direction at the γ/γ′ phase interface [19]. Additionally, irregular hexagonal-shaped dislocation networks developed at some γ/γ′ phase interfaces as indicated in Fig. 6c, as two sets of dislocations in octahedral slip planes interacted to form an alternate set of dislocations (i.e., $1/2[\bar{1}01] + 1/2[01\bar{1}] \rightarrow 1/2[\bar{1}10]$) by which the misfit strain could be relieved more efficiently [20]. Various dislocation networks induced sessile dislocation substructures, which might strengthen the alloy. Moreover, as observed in Fig. 6d, some bow-shaped dislocations moved around γ′ precipitates, displaying distinctly different morphologies. Occasionally, dislocations were observed to shear into the γ′ precipitates (Fig. 6d). By analyzing the features of dislocations, it can be concluded that dislocation glide and climb were the predominant deformation mechanisms for this alloy under LCF at 825 °C.

TEM images of microstructure and typical dislocation patterns for the [111]-oriented specimen tested at 825 °C are given in Fig. 7. The relative width of γ-matrix channels became slightly larger, compared to that for [001] orientation. The dislocation lines were mainly observed in the γ matrix, but with disordered patterns. As marked in Fig. 7a and

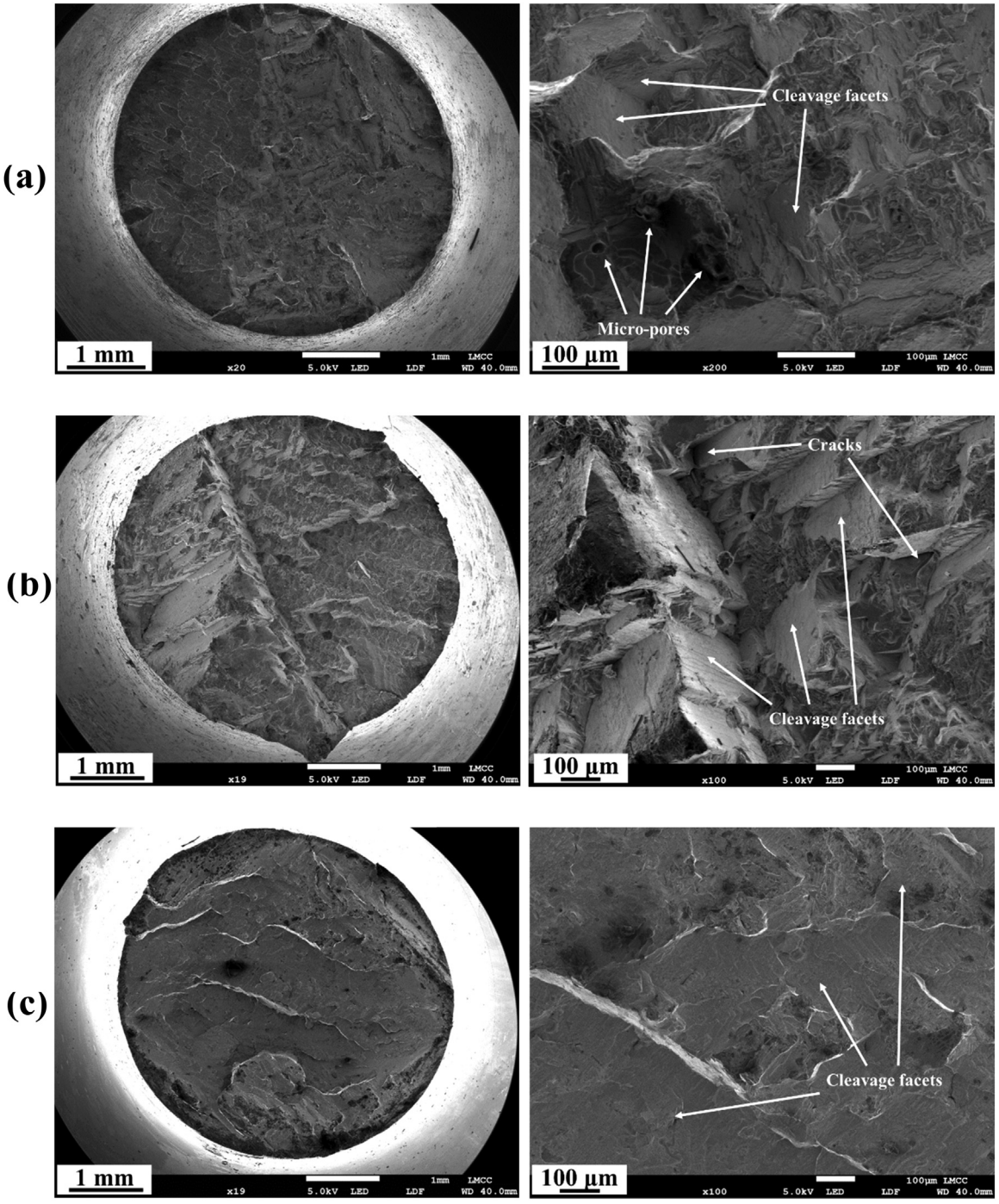


Fig. 4. Fractographs of fractured specimens: (a) [001] orientation at 825 °C; (b) [111] orientation at 825 °C; (c) [001] orientation at room temperature.

b, some short and straight dislocation lines were aligned in parallel, demonstrating high resistance to dislocation motion, which was not observed for [001] orientation. At 825 °C, dislocations could glide and climb to move between γ′ precipitates, as a result of high strength of the γ′ phase. Bow-like dislocations were observed to move around γ′ particles as shown in Fig. 7c, which was similar to the case for [001] orientation. The bow-shaped dislocation structures were caused by the evolution of dislocation segments around the cuboidal γ′ particles at the γ/γ′ interfaces [6]. In Fig. 7d, dislocations piled up at the γ/γ′ interfaces generating dislocation networks, which can accommodate the misfit strain, thereby releasing the misfit stress. Also, more zig-zag dislocations were also observed (Fig. 7e), indicating easier cross slip of dislocations for [111] orientation. The zig-zag dislocation configurations were generated by the cross slip of screw dislocations across the octahedral slip planes in horizontal γ channels, resulting in mixed 60° dislocation at the bottom and upper surfaces of the γ′ particle. Dislocation tangles got pinned in the γ channels with increasingly disordered patterns, making dislocations more difficult to move in the γ matrix and further promoting the shearing of dislocations into the γ′ precipitates (Fig. 7f). From these TEM observations, it can be concluded that dislocation cross-slip, in addition to glide and climbing, also became a major deformation mechanism for the [111]-oriented specimen tested at 825 °C.

Dislocation configurations in the [001]-oriented specimen tested in fatigue at room temperature are shown in Fig. 8. Apparently, dislocations also accumulated at the γ/γ′ interfaces, but with an overall density

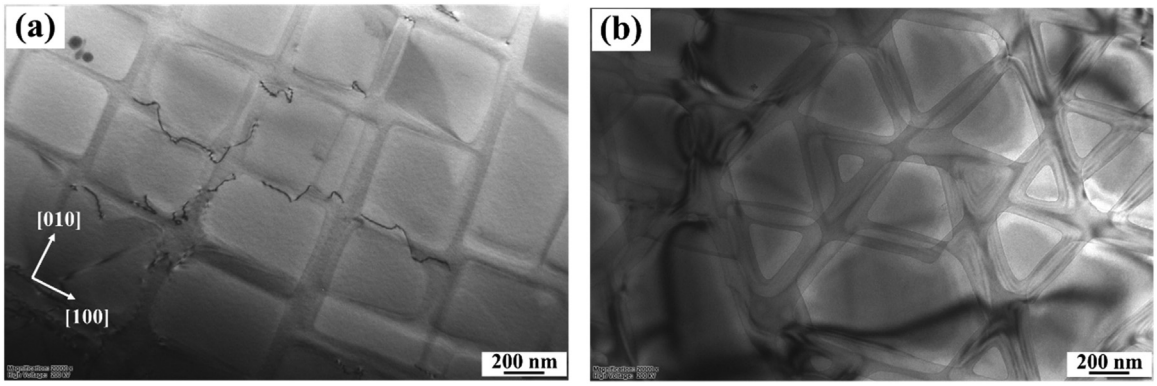


Fig. 5. Microstructure of as-received sample with (a) [001] and (b) [111] orientations.

lower than that at 825 °C (Figs. 6 and 7). With a decrease in temperature, the density of dislocations decreased with a reducing dislocation length. The process of dissolution of γ′ particles was very limited at room temperature when compared to that at 825 °C. The occasional cross-slip of screw-dislocation segments on the {111} slip planes in the horizontal γ matrix channels is illustrated in Fig. 8b, but without cross-slip movement. This indicates that it was more difficult for dislocations to cross over different {111} slip planes, with planar slip being the dominant deformation mechanism at room temperature [21,22]. Thus, when the dislocations evolved in the same slip plane, they formed highly tangled networks of dislocations in the γ channels as shown in Fig. 8c. In addition, inhomogeneity of dislocation distributions in the specimen can be observed in Fig. 8c, and some dislocations were occasionally observed to shear into the precipitates (Fig. 8d). The dislocation density was different across the specimen, and the bow-like dislocations moved around the γ′ particles (similar to the samples tested at 825 °C). For samples tested at room temperature, stacking faults was formed in the γ′ precipitates, as indicated in Fig. 8d and also further discussed in Section 4.3.

4. Discussions

4.1. Cyclic softening/hardening behaviour at 825 °C

At 825 °C, the [001]-oriented specimen exhibited cyclic softening at the initial stage of LCF, irrespective of the imposed strain amplitude (Fig. 3). First, the dissolution of γ′ precipitates at 825 °C led to cyclic softening at high temperature. From Fig. 6, the dissolution of the corners of γ′ precipitates is observed, compromising the cubic shape of original γ′ particles, thereby reducing the Orowan stresses required for dislocations to bow into the γ matrix channels. Also, interfacial misfit strains can result in progressive coarsening of the γ′ precipitates and widening of the γ channels, further decreasing the resistance to dislocation movement in the γ channels. During cyclic straining, γ′ precipitates were weakened due to the repeated shearing of the γ′ phase by dislocations, leading to a reduction of the ordered phases and resulting

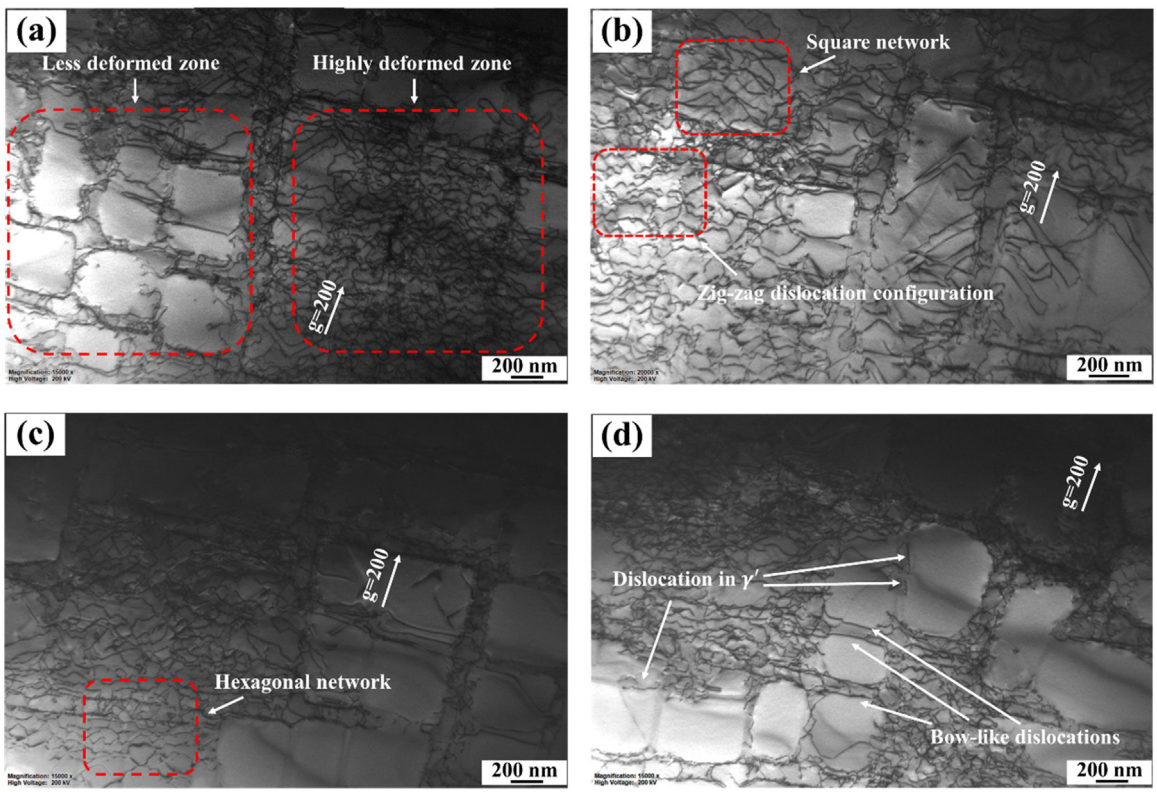


Fig. 6. TEM bright field (BF) micrographs showing dislocation configurations in fatigue-tested superalloy with [001] orientation at 825 °C.

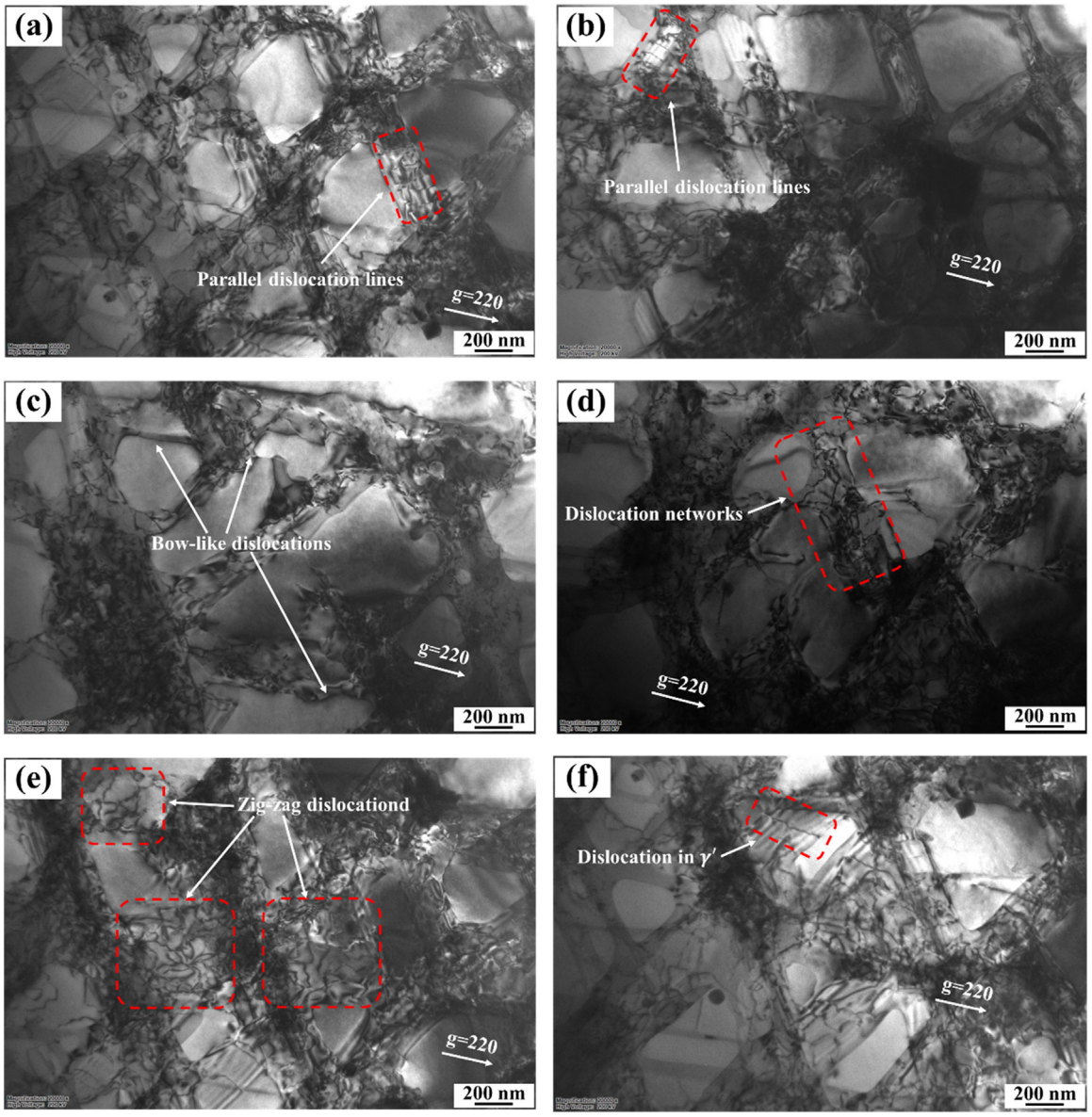


Fig. 7. TEM images showing dislocations in [111]-oriented specimen fatigue-tested at 825 °C.

in mechanical disordering. Softening and strain localisation was promoted by the destruction of ordered local atomic arrangements [21]. Furthermore, at high temperature, dislocations became more active in cross-slip and climb as a result of severe thermal activation and high relative intensity of γ/γ′ phases, causing a rapid development of dislocation networks at the γ/γ′ interfaces leading to the softening effect [23,24]. Meanwhile, dislocation annihilation occurred during fatigue, resulting in a reduction of the dislocation density within the deformed γ channels and a decrease of internal stresses. In conclusion, dissolution of γ′ particles, shearing of dislocations into γ′ precipitates, development of interfacial dislocation networks and dislocation recovery process were responsible for the initial cyclic softening behaviour of the [001]-oriented specimen tested at 825 °C.

The [111]-oriented specimen showed an initial cyclic hardening behaviour at 825 °C under low total strain amplitude (0.6%; Fig. 3). For the face-centred-cubic (FCC) structure, there are eight equivalent octahedral slip systems for the nominal [001] orientation, and six equivalent octahedral slip systems for the [111] orientation [25]. However, Vattré et al. [26] discussed that under low strain, eight octahedral slip systems were almost active equally for the [001] orientation, while the [111] orientation had only two octahedral slip systems active, although its six octahedral slip systems had the same Schmid factor. Thus, slip-system activation was an important factor that affected deformation at the low strain amplitude. The lack of slip-system activation was a cause of cyclic hardening for the [111]-oriented specimen. In addition, by comparing TEM observations with those for the [001]-oriented specimen (Fig. 6), many parallel arrays of dislocations were found to exist at the γ/γ′ interfaces for the [111]-oriented specimen (Fig. 7). The structure of parallel dislocation caused greater resistance to dislocation movement between different slip planes; as a result, dislocations favoured to slip in a single family of slip systems. Under higher strain amplitude (0.8%), the cyclic stress response of the [111]-oriented specimen exhibited an initial softening character (Fig. 3). TEM observations illustrated both the generation of dislocation networks and the dissolution of γ′ particles, indicating a similar softening mechanism for the [111]-oriented alloy.

4.2. Effect of temperature on LCF behaviour

For a given temperature, the fatigue life depends on key mechanical

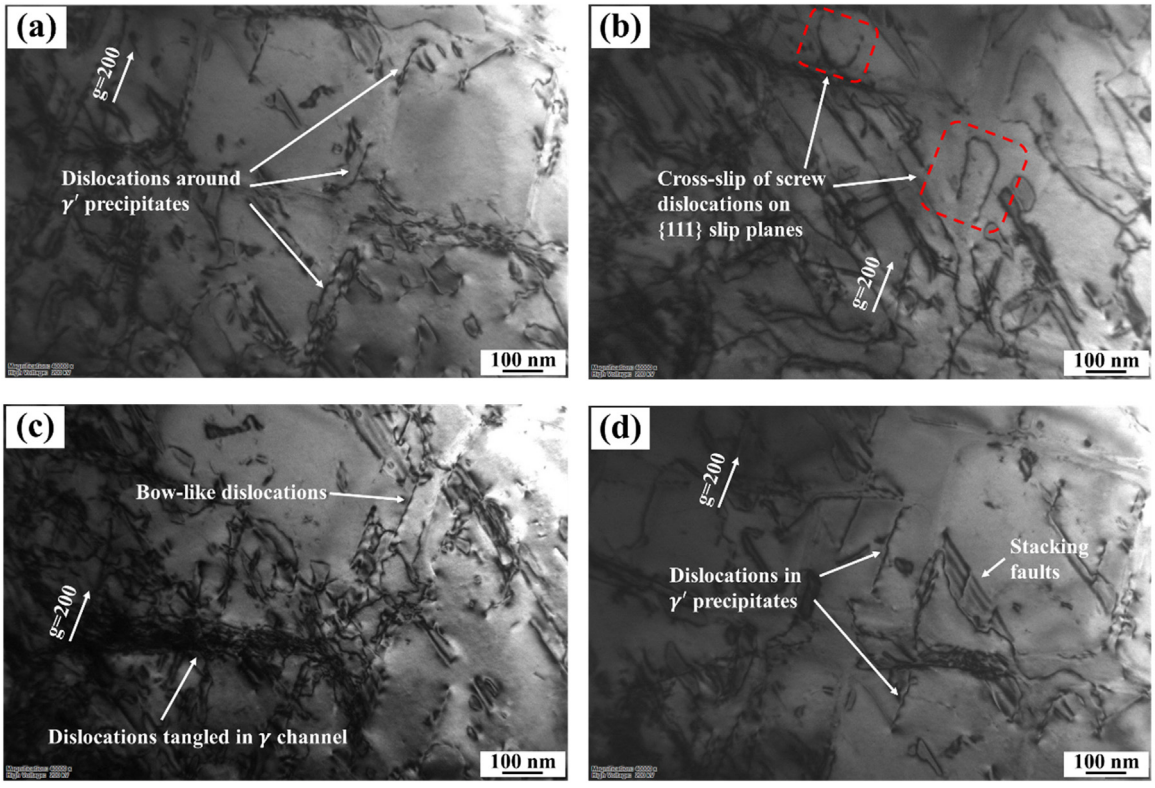


Fig. 8. TEM images showing the dislocations in [001]-oriented specimen tested at room temperature.

factors such as stress level, loading mode and temperature [27]. An increase in temperature leads to a reduction of the strength of γ′ precipitates, acceleration of an oxidation process and induction of the cyclic-slip irreversibility, thus resulting in microstructural damage of the alloy. Also, some key material parameters, such as the elastic modulus [6] and yield stress [28], can change with testing temperature, which can significantly influence the process of crack initiation and propagation. For the [001]-oriented specimen, the peak stresses at room temperature were higher than those at 825 °C under identical strain amplitude, and cyclic softening/hardening behaviour was found dependent on the testing temperature.

To further analyse the temperature-dependent material behaviour, a LCF test was carried out for the [111]-oriented specimen at room temperature at the same strain-controlled loading condition but interrupted at the 20th cycle under 0.8% strain amplitude when surface cracks appeared. The stress-strain response for the first cycle at each strain level (0.6% and 0.8%) is plotted in Fig. 9, together with evolution of the stress amplitude with the number of cycles. Comparing with the test at 825 °C (Figs. 2 and 3), the initial stress amplitude of the [111]-oriented specimen at room temperature was higher for both 0.6% and 0.8% strain amplitudes – 1108 MPa and 1436 MPa, respectively. Cyclic hardening was observed at 0.6% (Fig. 9b), similar to that at 825 °C (Fig. 3). However, the [111]-oriented specimen demonstrated continued cyclic hardening under 0.8% strain amplitude at room temperature rather than softening behaviour as observed at 825 °C. Compared to the [001]-oriented specimen tested at room temperature (Fig. 2), the area of hysteresis loops for [111]-oriented specimen was much larger, indicating higher plastic deformation (Fig. 9a). Besides, the peak stresses for the [111]-oriented specimen were higher than those for the [001]-oriented specimen at room temperature. The former specimen showed continuous cyclic hardening for both strain amplitudes (Fig. 9b); while the latter specimen demonstrated slight cyclic softening under 0.6% strain amplitude followed by cyclic hardening when the applied strain amplitude was subsequently increased to 0.8% and 1.0% at room temperature (Fig. 3).

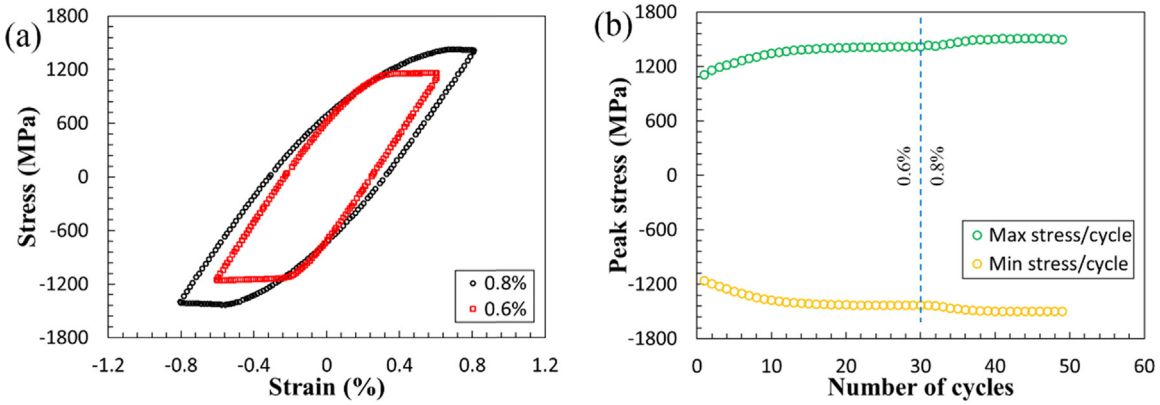


Fig. 9. Stress-strain loops for first cycle (a) and evolution of stress amplitude to failure (b) for [111]-oriented specimen tested at room temperature.

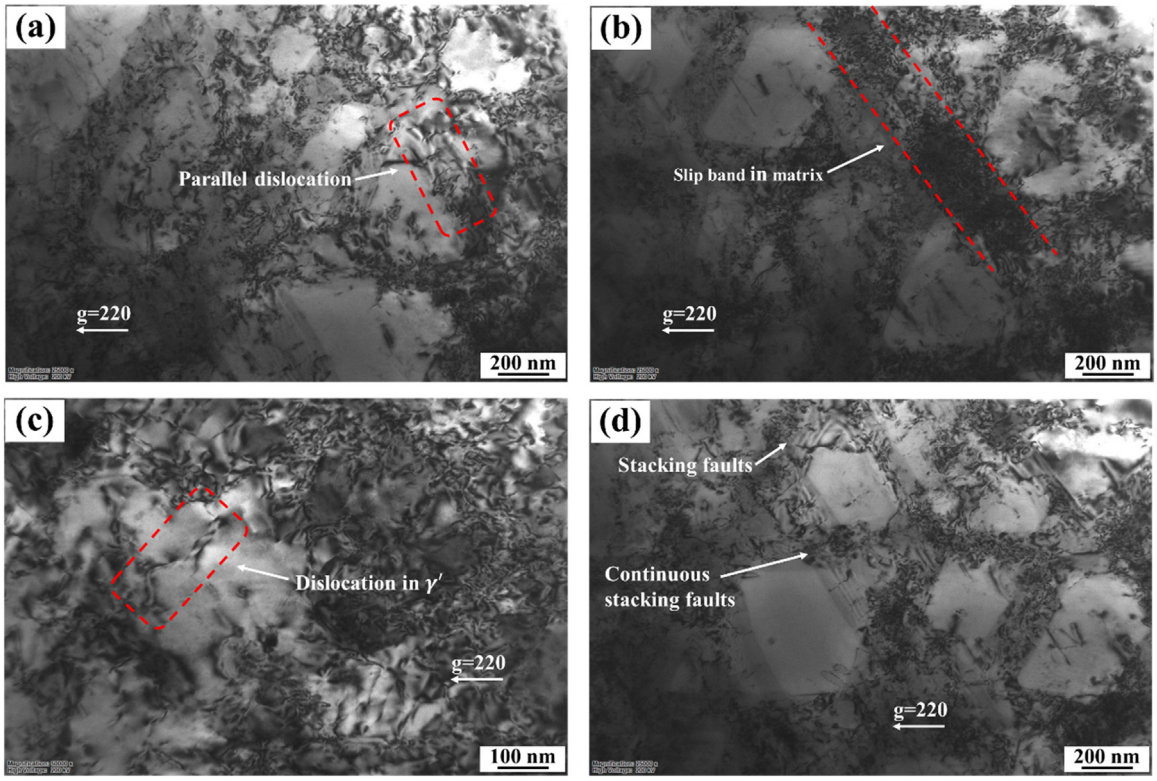


Fig. 10. TEM images showing dislocations in [111]-oriented specimen after LCF testing at room temperature.

4.3. Cyclic hardening at room temperature

Different from the cyclic stress response at 825 °C, both [001]- and [111]-oriented specimens exhibited only cyclic hardening under various strain levels at room temperature. The dislocation microstructure of the [111]-oriented sample tested at room temperature is illustrated in Fig. 10. It can be observed in Fig. 10a that γ′ precipitates were slightly dissolved and γ-matrix channels were widened, reducing the Orowan stress required for dislocations to bow out around the precipitates. In contrast, the parallel dislocation structures induced the higher resistance to dislocation movement and cyclic deformation. Therefore, the [111] orientation presented cyclic-hardening features during the early stage of LCF deformation. Only narrow slip bands were observed in γ channels (Figs. 8c and 10b), and shearing of γ′ precipitates by dislocations was not extensively present (Fig. 10c). The formation of irregular dislocation networks from partially misfit dislocations impeded the subsequent dislocation movement, leading to a cyclic hardening behaviour. As reported in Décamps et al. [29], the interfacial dislocation networks might hinder other dislocations from penetrating into the γ′ precipitates, thus leading to an absence of shearing of γ′ precipitates or material softening. Continuous stacking faults were present at room temperature (Figs. 8d and 10d). As suggested in Viswanathan et al. [30] and Décamps et al. [31], such faults were generated by the dissociation of a/2⟨110⟩ matrix dislocation and the subsequent shearing of γ′ precipitates by propagation of a leading partial dislocation. This mechanism is favoured when the stacking fault energy of the γ matrix or the width of the γ channel decreases and the applied stress increases [31]. Once stacking faults are formed, they act as barriers to dislocation movement, making plastic deformation more difficult, thereby contributing to cyclic hardening.

5. Conclusions

Strain-controlled cyclic deformation with varied strain amplitudes was studied for a nickel-based single-crystal superalloy, with a focus on the effects of orientation and temperature. The study was also supported by comprehensive TEM analyses. The alloy exhibited anisotropic behaviour during cyclic deformation. At 825 °C, the [001]-oriented specimen showed cyclic softening at the early stage of fatigue deformation, while the [111]-oriented specimen demonstrated cyclic hardening under lower strain level and cyclic softening under higher one. The fatigue life of the [111]-oriented specimen was significantly shorter than that of the [001]-oriented specimen. The initial cyclic softening behaviour for the [001]- and [111]-oriented specimens was caused by dissolution of γ′ precipitates, formation of interfacial dislocation networks and annihilation of dislocations. The cyclic hardening, especially at room temperature, was due to the formation of dislocations arrays that were aligned parallelly in γ matrix channels, preventing interactions of dislocation between different slip systems. The dislocation entanglement in the γ matrix, caused by gliding, cross-slip and dislocation climb, also contributed to the cyclic hardening by increasing the resistance of the material to cyclic plastic deformation.

Acknowledgements

This work was funded by the EPSRC (Grant EP/M000966/1 and EP/K026844/1) of the UK and in collaboration with GE Power, Rolls-Royce and dstl. The authors are grateful to Prof. Philippa Reed (University of Southampton) and Prof. Michael Preuss and Dr. João Quinta da Fonseca (University of Manchester) for several useful discussions of the results. We would also like to acknowledge the great support of Tsinghua University of China (Prof Changqing Chen and Dr Manqiong Xu) for the comprehensive TEM work. Research data for this paper is available on request from the project's principal investigator Professor Liguo Zhao at Loughborough University.

References

[1] P. Caron, T. Khan, Evolution of Ni-based superalloys for single crystal gas turbine blade applications, Aerosp. Sci. Technol. 3 (1999) 513–523.

[2] R.C. Reed, The Superalloys: Fundamentals and Applications, Cambridge University Press, New York, 2006.
[3] M. Segersäll, J.J. Moverare, Crystallographic orientation influence on the serrated yielding behavior of a single-crystal superalloy, Materials 6 (2) (2013) 437–444.
[4] E. Fleury, L. Remy, Low cycle fatigue damage in nickel-base superalloy single crystals at elevated-temperature, Mater. Sci. Eng. A 167 (1993) 23–30.
[5] Y. Li, X. Wu, H. Yu, B. Su, M. Zhang, Low cyclic deformation behavior of single crystal nickel base superalloys with different orientations at 980 °C, J. Chin. Electron Microsc. Soc. 33 (6) (2014) 15–18.
[6] L. Liu, J. Meng, J. Liu, T. Jin, X.D. Sun, H.F. Zhang, Effects of crystal orientations on the cyclic deformation behavior in the low cycle fatigue of a single crystal nickel-base superalloy, Mater. Des. 131 (2017) 441–449.
[7] M. Sundararaman, W. Chen, R.P. Wahi, A. Wiedenmann, W. Wagner, W. Petry, TEM and SANS investigation of age hardened nimonic PE16 after cyclic loading at room temperature, Acta Metall. Mater. 40 (1992) 1023–1028.
[8] S.G.S. Raman, K.A. Padmanabhan, Room temperature low cycle fatigue behaviour of Ni-base superalloy, Int. J. Fatigue 16 (1994) 209–215.
[9] M. Petrenec, K. Obrtlik, J. Polak, Inhomogeneous dislocation structure in fatigued INCONEL 713 LC superalloy at room and elevated temperatures, Mater. Sci. Eng. A 400- 401 (2005) 485–488.
[10] A. Pineau, S.D. Antolovich, High temperature fatigue of nickel-base superalloys - a review with special emphasis on deformation modes and oxidation, Eng. Fail. Anal. 16 (2009) 2668–2697.
[11] Z.K. Chu, J.J. Yu, X.F. Sun, H.R. Guan, Z.Q. Hu, High temperature low cycle fatigue behavior of a directionally solidified Ni-base superalloy DZ951, Mater. Sci. Eng. A 488 (2008) 389–397.
[12] S. Volker, F.K. Monika, Orientation dependence of dislocation structures and deformation mechanisms in creep deformed CMSX-4 single crystals, Mater. Sci. Eng. A 245 (1998) 19–28.
[13] J.J. Yu, X.F. Sun, T. Jin, N.R. Zhao, H.R. Guan, Z.Q. Hu, High temperature creep and low cycle fatigue of a nickel-base superalloy, Mater. Sci. Eng. A 527 (2010) 2379–2389.
[14] T.P. Gabb, G. Welsch, The high-temperature deformation in cyclic loading of a single-crystal nickel-base superalloy, Acta Metall. 37 (1989) 2507–2516.
[15] X.G. Wang, J.L. Liu, T. Jin, X.F. Sun, Y.Z. Zhou, Z.Q. Hu, J.H. Do, B.G. Choi, I.S. Kim, C.Y. Jo, Deformation mechanisms of a nickel-based single-crystal superalloy during low-cycle fatigue at different temperatures, Scr. Mater. 99 (2015) 57–60.
[16] S. Li, L. Ping, Low-cycle fatigue behavior of a nickel base single crystal superalloy at high temperature, Rare Metal. Mater. Eng. 44 (2) (2015) 288–292.
[17] B. Lin, M.S. Huang, L.G. Zhao, A. Roy, V. Silberschmidt, N. Barnard, M. Whittaker, G. McColvin, 3D DDD modelling of dislocation–precipitate interaction in a nickel-based single crystal superalloy under cyclic deformation, Philos. Mag. 98 (2017) 1550–1575.
[18] Z.L. Zhan, J. Tong, A study of cyclic plasticity and viscoplasticity in a new nickel-based superalloy using unified constitutive equations. Part I: evaluation and determination of material parameters, Mech. Mater. 39 (2007) 64–72.
[19] J. Zhang, J. Wang, H. Harada, Y. Koizumi, The effect of lattice misfit on the dislocation motion in superalloys during high-temperature low-stress creep, Acta Mater. 53 (2005) 4623–4633.
[20] Z.P. Luo, Z.T. Wu, D.J. Miller, The dislocation microstructure of a nickel-base single-crystal superalloy after tensile fracture, Mater. Sci. Eng. A 354 (2003) 358–368.
[21] R.E. Stoltz, A.G. Pineau, Dislocation-precipitate interaction and cyclic stress-strain behavior of a γ' strengthened superalloy, Mater. Sci. Eng. 34 (1978) 275–284.
[22] B.A. Lerch, V. Gerold, Cyclic hardening mechanisms in NIMONIC 80A, Metall. Mater. Trans. A 18 (1987) 2135–2141.
[23] K.B.S. Rao, H. Schiffers, H. Schuster, Influence of time and temperature-dependent processes on strain controlled low-cycle fatigue behavior of alloy-617, Metall. Mater. Trans. A. 19 (1988) 359–371.
[24] M.R. Daymond, M. Preuss, B. Clausen, Evidence of variation in slip mode in a polycrystalline nickel-base superalloy with change in temperature from neutron diffraction strain measurements, Acta Mater. 55 (2007) 3089–3102.
[25] M. Segersäll, D. Leidermark, J.J. Moverare, Influence of crystal orientation on the thermomechanical fatigue behaviour in a single-crystal superalloy, Mater. Sci. Eng. A 623 (2015) 68–77.
[26] A. Vattré, B. Devincre, A. Roos, Orientation dependence of plastic deformation in nickel-based single crystal superalloys: discrete–continuous model simulations, Acta Mater. 58 (2010) 1938–1951.
[27] J.E. King, Fatigue crack propagation in nickel-base superalloys - effects of microstructure, load Ratio, and temperature, Mater. Sci. Technol. 3 (1987) 750.
[28] Y.M. Wang-Koh, Understanding the yield behaviour of $L1_2$-ordered alloys, Mater. Sci. Technol. 33 (8) (2017) 934–943.
[29] B. Décamps, V. Brien, A.J. Morton, Deformation microstructures after low-cycle fatigue at 950 °C in Ni-based superalloys: the effect of test conditions, Scr. Metall. Et. Mater. 31 (1994) 793–798.
[30] G.B. Viswanathan, P.M. Sarosi, M.F. Henry, D.D. Whitis, W.W. Milligan, M.J. Mills, Investigation of creep deformation mechanisms at intermediate temperatures in René 88 DT, Acta Mater. 53 (2005) 3041–3057.
[31] B. Décamps, A.J. Morton, M. Condat, On the mechanism of shear of γ′ precipitates by single (a/2)⟨110⟩ dissociated matrix dislocations in Ni-based superalloys, Philos. Mag. A 64 (1991) 641–668.